POD as tool for comparison of PIV and LES data

Meyer, Knud Erik; Cavar, Dalibor; Pedersen, Jakob Martin

Published in:
7th International Symposium on Particle Image Velocimetry

Publication date:
2007

7th International Symposium on Particle Image Velocimetry
Rome, Italy, September 11–14, 2007

POD as tool for comparison of PIV and LES data

Knud Erik Meyer, Dalibor Cavar and Jakob M. Pedersen
Department of Mechanical Engineering, Technical University of Denmark
Building 403, DK-2800 Lyngby, Denmark, e-mail: kem@mek.dtu.dk

Abstract Both Particle Image Velocimetry (PIV) and Large Eddy Simulation (LES) provides instantaneous velocity fields which can contain dynamical flow structures that occur systematically. Turbulent flows also contain random flow structures, and therefore there is a need for tools that can identify the systematic dynamic flow structures. We show how Proper Orthogonal Decomposition (POD) based on snapshots (instantaneous flow realizations) can be used for this purpose. As a test case, we use PIV measurements and LES calculations on the same turbulent jet in cross flow. The Reynolds number based on the crossflow velocity and pipe diameter is 2400 and the jet to crossflow velocity ratio is $R = 3.3$. The POD is able to identify two dynamic flow structures: jet shear-layer vortices and wake vortices. A good agreement for the dynamical content is found between PIV and LES.

1 Introduction

Particle Image Velocimetry (PIV) provides instantaneous velocity vectors in a plane and offers new possibilities compared to traditional point-based techniques. For numerical simulations, a similar change from point-based statistics (Reynolds Averaged Numerical Simulation, RANS) to Large Eddy Simulation (LES) is taking place. However, comparison of LES results to experiments relies still in most cases on point-based time-averaged statistics. There is a need for tools that can compare the dynamical content in PIV measurements and LES calculations, respectively. For turbulent flows, the comparison must be done on a statistical basis. We will demonstrate how Proper Orthogonal Decomposition (POD) can be used as such a tool.

We will use the jet in crossflow as an example. This flow is a common way to mix two fluids. Practical examples are control of combustion by the so-called "over fire air" in large boilers, mixing of gases before chemical reactions in e.g. air pollution control systems and designs for film cooling in gas turbines. The flow has a simple geometry, but the resulting flow is quite complex. Visualization studies, e.g. [1, 2, 3] have shown a number of flow structures. Figure 1(a) show these structures as as presented in [4]. Some structures have mean flow definition: the counter rotating vortex pair (CVP) created below the trajectory of the jet, one or more horseshoe vortices found upstream of the jet exit and the hanging vortices. There are at least two important non-stationary flow structures. The first one is that of jet shear-layer vortices formed especially along the upstream side but also at the lee-side of the jet as a result an instability similar to the Kelvin-Helmholtz instability. The second unsteady structure is that of upright vortices or wake vortices found as vertical vortices moving downstream in the wake of the jet. The unsteady structures do not show up in the mean field. We will look for these structures when we investigate POD as a method to identify dynamical structures statistically.

The visualization studies by [1, 2, 3] all use laminar in-flow conditions with thin boundary layers. This creates very regular flow structures that are easy to visualize and to describe. Most

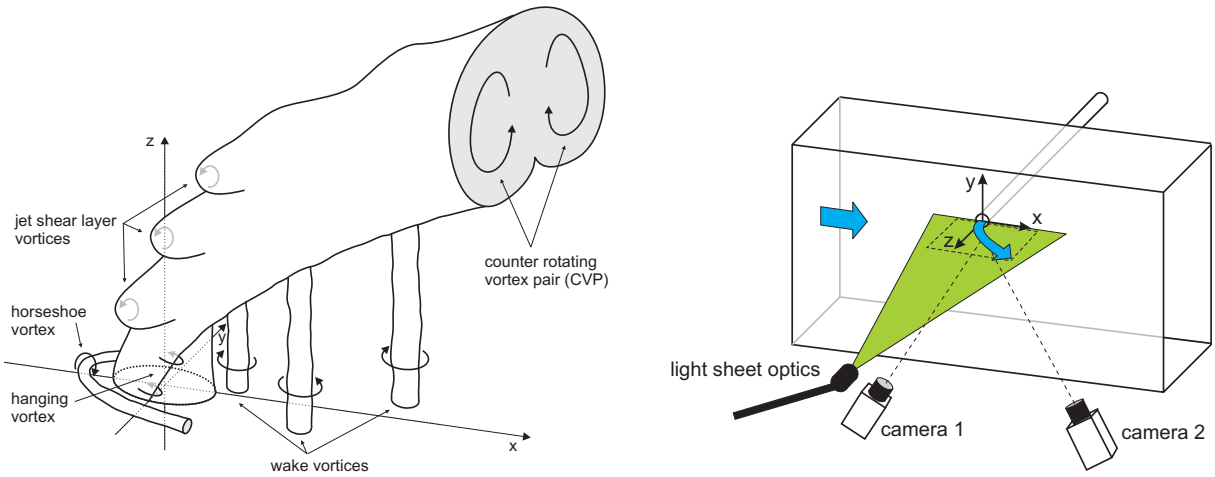

(a) (b)

Figure 1: Schematic description of vortical structures in the jet in crossflow near jet exit (a) and a sketch of the experimental setup (b).

real applications of a jet in cross flow have turbulent inflow conditions. This makes visualization using tracers much more difficult both in physical experiments and in numerical calculations. This stresses the need for other tools for analysis of dynamic flow structures.

In the following section, we briefly present the experimental setup and method, the numerical calculations, the Proper Orthogonal Decomposition (POD) and finally, we show and discuss results.

2 Experimental setup

A jet from a turbulent pipe flow issued into a turbulent boundary layer in a low-speed wind tunnel, see figure 1(a). The wind tunnel has a cross section of 600 mm $\times$ 264 mm and the jet exit was located 1350 mm downstream of tripping devices that made the boundary layer turbulent. The thickness of the boundary layer at the jet exit was measured to be $\delta_{99\%} = 70$ mm. The jet was discharged from a 2.5 m long pipe with diameter $D = 24$ mm and measurements indicated fully turbulent flow. The Reynolds number based on the crossflow velocity and pipe diameter is 2400 and the jet to crossflow velocity ratio is $R = 3.3$. The measurements were done in many different planes, but only two planes are included in the present paper: the $y = 0$ plane and the $z = 1.33D$ plane.

The stereoscopic PIV system consisted of two Kodak Megaplus ES 1.0 cameras (resolution of 1008×1016) with 60 mm Nikkor lenses mounted in the Scheimpflug condition. The angle between the cameras was approximately 80° and the recordings used an F-number of 2.8. The light sheet of thickness 1.5 mm was created with a double cavity Nd-YAG laser delivering 100 mJ light pulses. The configuration of cameras and light sheet for measurements in constant y-planes is illustrated in figure 1(b). For measurements in z-constant planes, the positions of cameras and laser sheet optics were interchanged. Seeding consisting of 2-3 μm droplets of glycerol was added to both the main flow and the jet.

The images were processed with Dantec Flowmanager version 3.4 using adaptive velocity correlation to a final resolution of 32x32 pixels per interrogation area using 25 percent overlap between interrogation areas. A calibration target aligned with the light sheet plane was used to

obtain the geometrical information required for the reconstruction of the velocity vectors. Image maps were recorded with an acquisition rate of 0.5 Hz, which ensured statistical independence of samples. For each plane, 1000 snapshots were acquired. The velocity vector maps contained typically 33 by 37 vectors. The linear dimensions of the interrogation areas varied between 1.5 and 3 mm.

3 Large Eddy Simulation

The eddy-viscosity based LES calculations have been performed utilizing the in-house flow solver EllipSys [5, 6], which is a multi-block finite volume solver for incompressible Navier-Stokes equations in general curvilinear coordinates. The code uses a collocated variable arrangement, where a revised Rhie/Chow interpolation is used to avoid odd/even pressure coupling. The pressure-velocity coupling is obtained by applying the well-known PISO algorithm. The solution is advanced in time using a 2nd order iterative time stepping (dual-time stepping). The EllipSys code is parallelized with MPI message parsing library for execution on distributed/shared memory machines by a non-overlapping domain decomposition technique.

The computational domain considered in LES calculations consists of a spanwise region ($12D$ - periodical boundary condition applied), two regions upstream the intersection point ($5D$ on the boundary layer side and $3D$ on the pipe side - inlet boundary condition), a region downstream of the intersection point ($12D$ - outlet boundary condition) and the wall normal region ($10D$ - wall and symmetry boundary condition applied on the bottom and top domain side respectively). Two separate precursor computations have been performed in order to obtain suitable turbulent inlet boundary conditions - one simulating a fully developed pipe flow and the other simulating spatially developing boundary layer flow. The latter flow is simulated utilizing the method of [7].

The SGS stresses are modeled through the eddy-viscosity assumption employing a Mixed Scale Eddy-Viscosity model of [8]. The convective terms in the Navier-Stokes equations are discretized utilizing the QUICK scheme to avoid a wiggle contamination of the instantaneous flow snapshots. The grid consists of app. 4.7 million cells. Disregarding the "*direct jet zone*", the grid can be described as a 200x120x120 cells grid in the streamwise, spanwise and wall-normal directions respectively - app. 2.9 million cells, whereas the *direct jet zone* is additionally covered by app. 1.8 million cells. Actually 14 different cases, where influence of various parameters (discretization schemes - CDS(4) vs. QUICK, domain inlet-outlet extensions, time step size, SGS eddy viscosity models - Smagorinsky, Dynamic Smagorinsky vs. Mixed Scale Eddy-Viscosity model of [8] etc.) have been investigated and grids of up to 14.8 million cells in size have been considered (for details see [9]) but none of them were able to better reproduce the measurements of [10] than the results presented in the following.

The POD analysis has been conducted on a dataset consisting of 1000 instantaneous flow snapshots extracted equidistantly in time during the total computational period of $270\ D/U_\infty$. The LES dataset contains only app. 90 statistically uncorrelated samples. The initial analysis was conducted on these 90 uncorrelated flow realizations showing qualitatively similar results to those based on 1000 samples. The main difference was that some structures were significantly "*blurred*" and not easily identifiable in the small dataset analysis. So despite the fact that the LES dataset contained statistically correlated data, it was decided to conduct the main LES analysis on the full dataset in order to accommodate comparison of PIV and LES data up to a similar level of detail.

4 Proper Orthogonal Decomposition on snapshots

The Proper Orthogonal Decomposition was first introduced in the context of fluid mechanics by Lumley [11]. The present analysis uses the so-called "snapshot POD" by Sirovich [12]. Here, each instantaneous PIV measurement is considered to be a snapshot of the flow. An analysis is then performed on typically 1000 snapshots taken in the same plane. The first step is to calculate the mean velocity field. The mean velocity field can be considered the zeroth mode of the POD. The rest of the analysis works on the fluctuating parts of the velocity components (u_j^n, v_j^n, w_j^n) where u, v and w denote the fluctuating part of each of the three velocity components. Index n runs through the N snapshots and j runs through the M positions of velocity vectors in a given snapshot (i.e. $u_j = u(x_j, y_j, z_j)$). All fluctuating velocity components from the N snapshots are arranged in a matrix $\mathbf{U}$ as

$$\mathbf{U} = [\mathbf{u}^1\ \mathbf{u}^2\ \ldots\ \mathbf{u}^N] = \begin{bmatrix} u_1^1 & u_1^2 & \ldots & u_1^N \\ \vdots & \vdots & \vdots & \vdots \\ u_M^1 & u_M^2 & \ldots & u_M^N \\ v_1^1 & v_1^2 & \ldots & v_1^N \\ \vdots & \vdots & \vdots & \vdots \\ v_M^1 & v_M^2 & \ldots & v_M^N \\ w_1^1 & w_1^2 & \ldots & w_1^N \\ \vdots & \vdots & \vdots & \vdots \\ w_M^1 & w_M^2 & \ldots & w_M^N \end{bmatrix} \tag{1}$$

The autocovariance matrix is created as

$$\widetilde{\mathbf{C}} = \mathbf{U}^T\mathbf{U} \tag{2}$$

and the corresponding eigenvalue problem

$$\widetilde{\mathbf{C}}\mathbf{A}^i = \lambda^i\mathbf{A}^i \tag{3}$$

is solved. The solutions are ordered according to the size of the eigenvalues

$$\lambda^1 > \lambda^2 > \ldots > \lambda^N = 0 \tag{4}$$

The eigenvectors of (3) make up a basis for constructing the POD modes $\boldsymbol{\phi}^i$,

$$\boldsymbol{\phi}^i = \frac{\sum_{n=1}^{N} A_n^i \mathbf{u}^n}{\left\| \sum_{n=1}^{N} A_n^i \mathbf{u}^n \right\|}, \qquad i = 1, \ldots, N \tag{5}$$

where A_n^i is the n'th component of the eigenvector corresponding to λ^i from eq. (3) and the discrete 2–norm is defined as

$$\|\mathbf{y}\| = \sqrt{y_1^2 + y_2^2 + \ldots + y_M^2}$$

Each snapshot can be expanded in a series of the POD modes with expansion coefficients a_i for each POD mode i. The coefficients, also called POD coefficients, are determined by projecting the fluctuating part of the velocity field onto the POD modes

$$\mathbf{a}^n = \boldsymbol{\Psi}^T\mathbf{u}^n \tag{6}$$

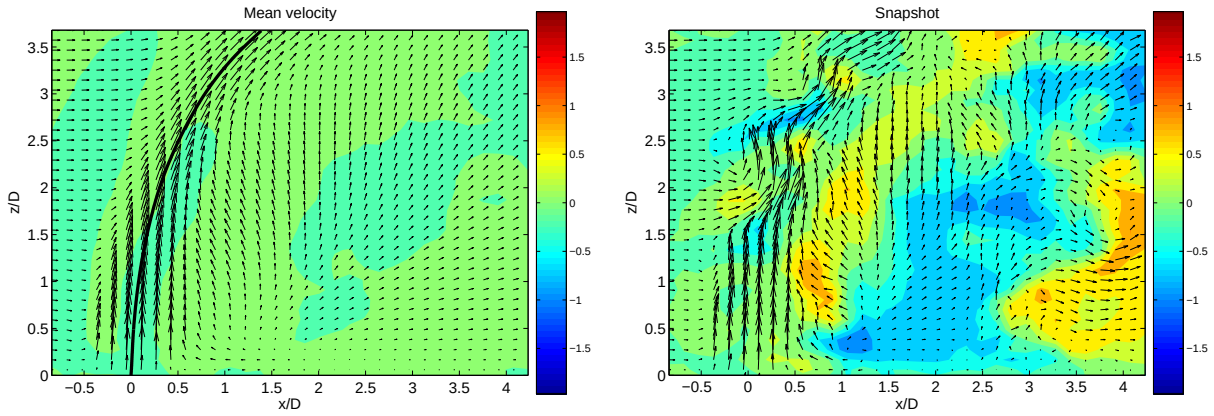

Figure 2: Mean velocity and a snapshot in the $y = 0$ plane.

where $\mathbf{\Psi} = [\boldsymbol{\phi}^1\ \boldsymbol{\phi}^2\ \ldots\ \boldsymbol{\phi}^N]$ has been introduced. The expansion of the fluctuating part of a snapshot n reads

$$\mathbf{u}^n = \sum_{i=1}^{N} a_i^n \boldsymbol{\phi}^i = \mathbf{\Psi}\mathbf{a}^n \tag{7}$$

It can be shown [13] that the amount of the total kinetic energy from velocity fluctuations in the snapshots that is associated with a given POD-mode is proportional to the corresponding eigenvalue. The ordering of the eigenvalues and eigenvectors in eq. (4) therefore ensures that the most important modes in terms of energy are the first modes. This usually means that the first modes will be associated with large scale flow structures. If a flow has dominant flow structures, these are therefore reflected in the first POD modes and hence a given snapshot can often be reconstructed satisfactorily using only the first few modes. More details on the POD can be found in [14] and [15]. The snapshot POD was made using the computing language MATLAB™. Each of eqs. (1)–(7) is typically expressed as a single line of script code.

5 Results

An overview of the flow can be seen in figure 2. All plots of vector fields in this paper use the background color to show the out-of-plane component. Velocities have all been normalized with the freestream velocity U_∞. The vectors in the plots show the in-plane components. Within each plot, the same scale has been used for both vectors and colors. The solid black line shows the jet trajectory found as a streamline released in the center of the jet exit.

Figure 2 shows the $y = 0$ plane, which contains the center part of the jet as it bends into the crossflow. The figure is also a good illustration of the difference between time-averaged statistics and instantaneous vector fields - which we will call “snapshots”. The mean field could just as well have been measured with a point method like Laser Doppler Anemometry. This type of data does not reveal two important flow structures that can be seen in the snapshot. The first structure is seen as a wavy pattern in the bended jet for $z/D > 1.5$. This is the jet shear-layer vortices. The second structure is seen in the wake behind the bended jet as regions of positive and negative out-of-plane components. This pattern is consistent with upright vortices in the wake, which we will call wake vortices.

Figure 3 shows a three-dimensional snapshot of the LES. The flow has been visualized using the Q-criterion of Hunt *et al* [16]. Positive values of Q have been found to identify vortices and the structures seen in figure 3 can therefore be interpreted as vortices. The pattern of vortices is

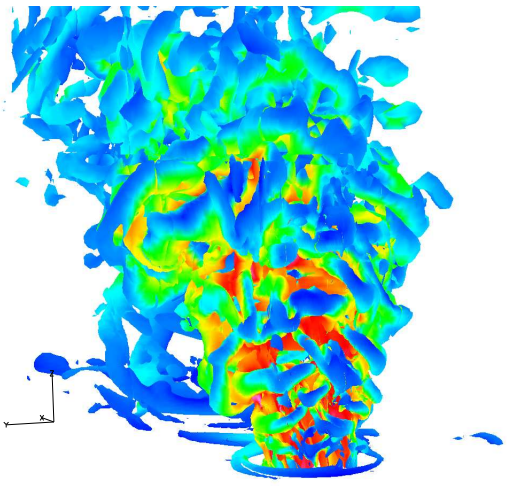

Figure 3: LES snapshot shown as iso-surfaces of Q-criterion colored with velocity magnitude.

quite chaotic and this is typical for turbulent flows. It is possible to identify horizontally aligned vortices in the front of the jet that probably are the jet shear-layer vortices. It is also possible for find vertically aligned vortices in the jet wake that probably are wake vortices. However, the visualization in figure 3 offers little help to distinguish between systematic and random flow patterns.

The traditional method to compare e.g. measurements and calculations is to use line-plots of components of mean velocities, RMS values or similar quantities. An example of such a plot is shown in figure 4. The mean velocity component in the cross flow direction U_M is plotted along vertical lines in the $y = 0$ plane. The $x/D = -1.0$ station shows the incoming boundary layer profile, lines near $x = 0$ shows relatively complex patterns in the jet core and the plot in the wake region ($x/D = 0.83$) shows a very complex variation of U_M. Outside the jet core, the agreement between calculations and measurements is quite good, but in the jet core a significant deviation is seen. The difference can be caused by several different effects: fundamental differences in the flow solutions, difference in inlet conditions (a slightly wrong velocity ratio R can create difference in jet bending) or difference caused by resolution of the solution (size of measurement volume or calculation grid). An analysis of dynamical content in the solutions can be helpful in this analysis.

The Proper Orthogonal Decomposition (POD) is a candidate for such an analysis of dynamical content. Figure 5 shows the results of a POD analysis of 1000 snapshots from the $y = 0$ plane. The results are shown as POD modes. The POD modes must be multiplied by its corresponding POD-coefficient and added to the mean flow (as shown in figure 2) to represent a real snapshot of the flow. The percentage of the total kinetic energy associated with each mode is indicated above each plot. The first observation from figure 5 is that the modes from PIV and LES are in very good qualitative agreement. Modes 1 and 2 are different from the following modes. Modes 1 and 2 have almost no in-plane component, but large out-of-plane component in the region behind the jet trajectory. The regions are consistent with large vortices in the wake region with vortex axes parallel to the jet trajectory. We interpret these modes as representing the wake vortices.

Mode 4 shows vortices moving along the jet trajectory. Adding this mode to the mean field results in a pattern near the jet trajectory similar to the pattern seen on the snapshot in figure 2.

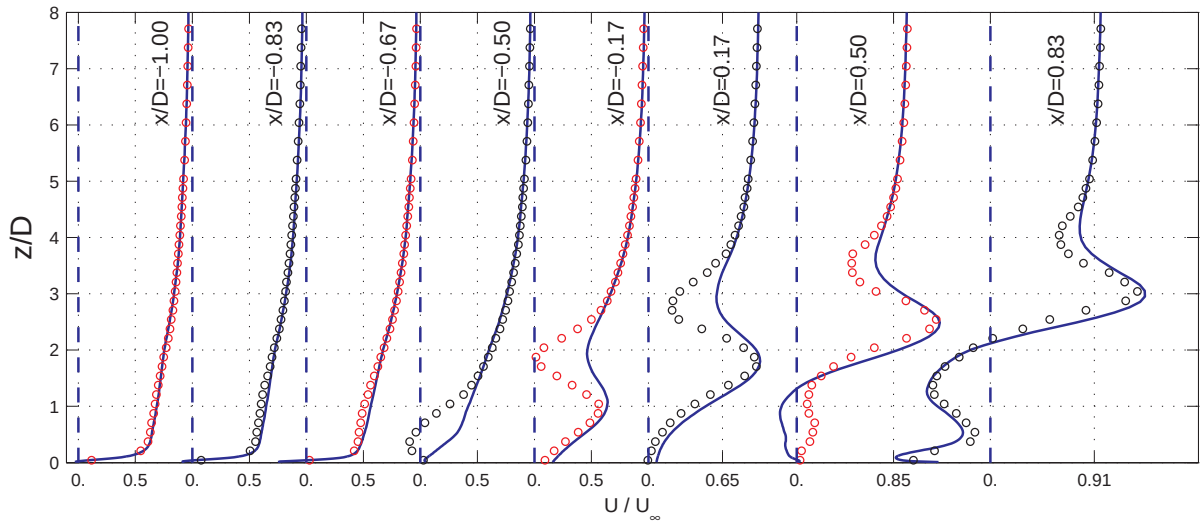

Figure 4: Mean velocity U/U_∞ at the $y = 0$ plane. Solid lines are LES and circles are LDA data from [10].

Our interpretation is that this mode represents the jet shear-layer vortices. A closer inspection of the mode 4 plots reveals that the vortices shown by the vectors are not at exactly the same position on the plots from from PIV and LES, respectively. The mode 5 plot (not shown) for PIV is almost identical to the mode 4 plot for LES. Likewise, the mode 5 plot for LES is almost identical to the mode 4 plot for PIV. The shift in positions illustrates that the positions of the vortices are arbitrary and that a snapshot with jet shear-layer vortices can be reconstructed using a combination of mode 4 and mode 5. The shift in positions of vortices is also found for the wake vortices in mode 1 and 2. For both PIV and LES, mode 3 (not shown) consist of in-plane vectors in near the jet trajectory that results in a change of the degree of bending of the jet.

POD modes 1 and 2 have for both PIV and LES significantly higher energy content associated than modes 3–5, which each have 3% of the total kinetic energy associated. This is partly because the velocity fluctuations for mode 1 and 2 cover a larger region than the fluctuations in modes 3–5. The energy associated with mode 1 and 2 is about 11% for each mode for PIV while it is about 8% for each mode for LES. A reason for this could be that the PIV measurements use an interrogation area that is larger than the smallest scales of velocity variations. The PIV measurements do therefore not measure the full content of turbulent kinetic energy in the flow. LES does also not (due to the basic idea in LES) resolve all turbulence kinetic energy. However, the computational grid for the LES is more detailed than the PIV measurement and is therefore likely to capture more of the turbulent velocity fluctuations. This is indeed the case as demonstrated in [9]. This explains why the relative content of energy in the two first modes are larger for PIV than for LES.

Figure 6 shows the mean field and POD modes for the $z = 1.33D$ plane. The mean fields are practically identical for PIV and LES. The jet core has been deformed in a semi-circular shape and two vortices are seen in the wake of the jet core. These are similar to the vortices found in the mean field behind a circular cylinder in cross flow. As for the cylinder in crossflow, the vortices in the mean flow field are just traces of the instantaneous vortices that are shed in the wake. However, the shedding process has important differences for a cylinder and a jet in crossflow, respectively, since the sources of vorticity are different: for a cylinder in crossflow, the vorticity is created at the cylinder wall while the vorticity in the jet in crossflow comes from

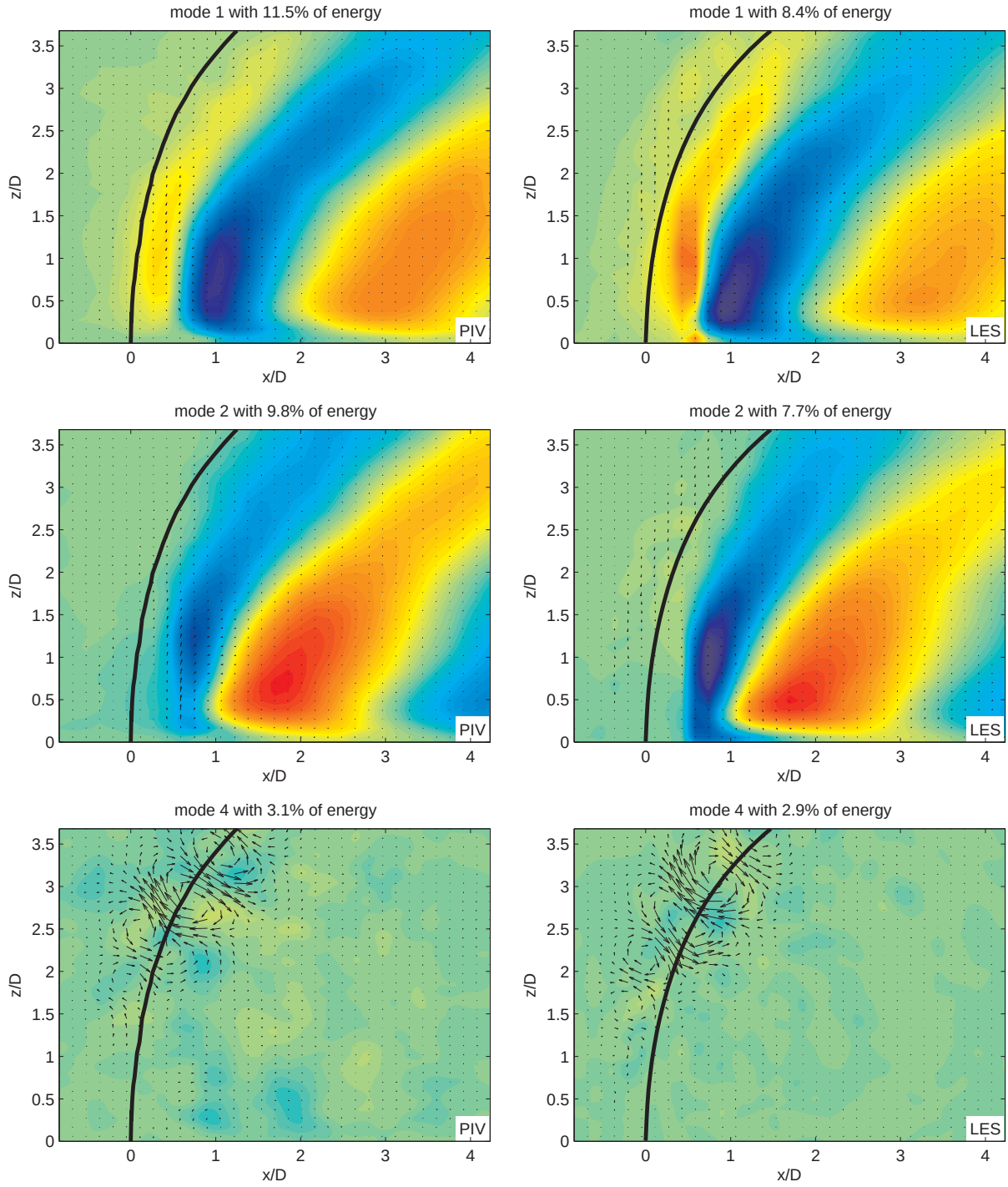

Figure 5: POD modes from PIV measurement (left) and from LES calculations (right) in the $y = 0$ plane.

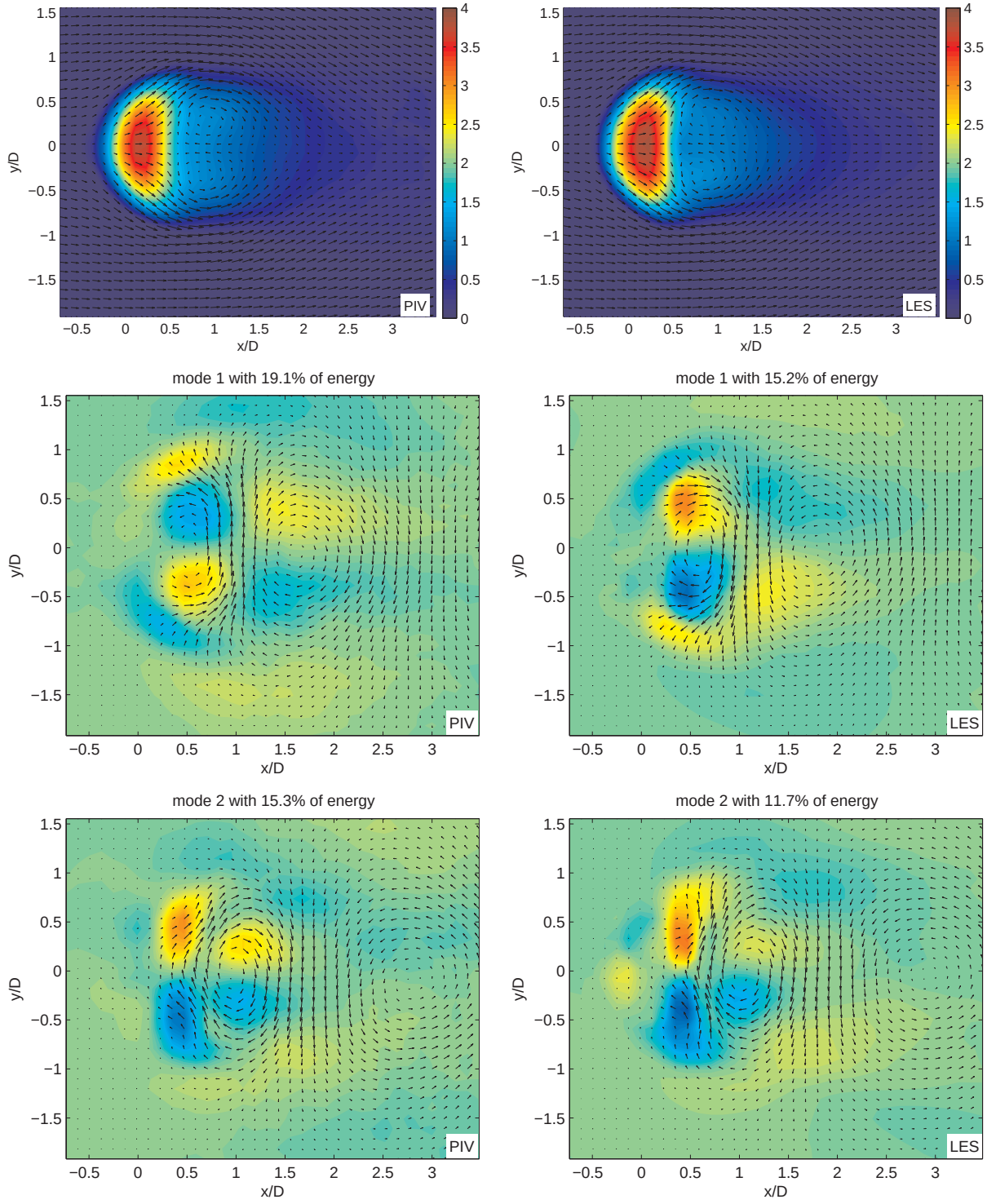

Figure 6: Mean flow field (top) and POD modes from PIV measurement (left) and from LES calculations (right) in the $z = 1.33D$ plane.

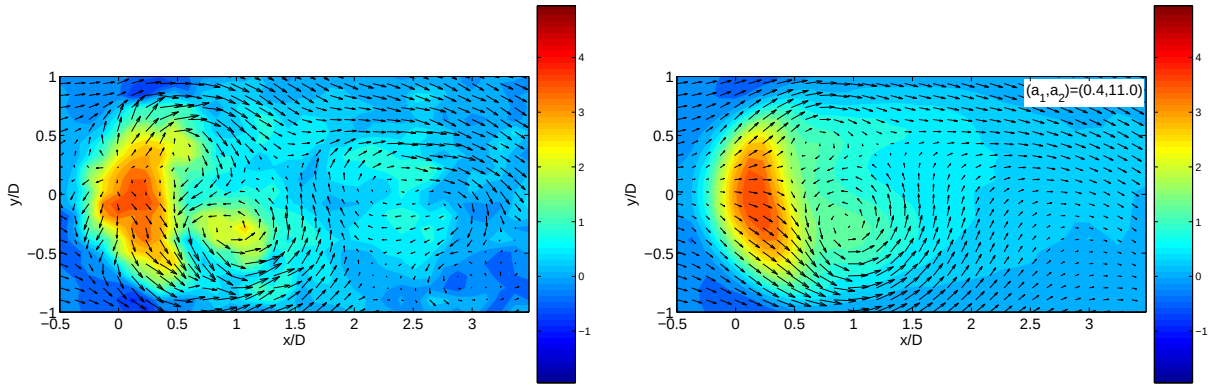

Figure 7: PIV snapshot (left) in the $z = 1.33D$ plane and the reconstruction using the two first POD modes.

the crossflow and jet boundary layers.

The POD modes in figure 6 have good qualitative agreement between PIV and LES. However, mode 1 for PIV needs a change of sign on all component to match the mode 1 for LES. Since POD modes are multiplied with constants found from eq. (6), the sign of a mode is not significant. The results for mode 1 for PIV and LES are therefore consistent with each other. Mode 1 and 2 have similar energy content. Mode 3 and following modes (not shown) have much less energy (3% or less) and represent variations from from the two first modes e.g. in the form of asymmetries.

Two patterns are seen. In the wake region, the in-plane vectors show a large vortex near $x/D = 1.5$ for mode 1 and two vortices for mode 2: one with center at $x/D = 1$ and one further downstream at $x/D = 3$. We assume that this pattern shows how wake vortices move downstream. The second pattern is regions of positive and negative out-of-plane motion in the jet core region. Since the modes are added to the mean flow, the effect of the patterns are to change the shape and position of jet core. The fact that these two patterns are seen in the same POD modes shows that the formation of the jet vortices is associated with significant sidewards movements of the jet core.

It is also interesting to compare the POD modes in figures 5 and 6 along the intersecting line between the two planes. The variations of the velocity component in the y-direction are in good qualitative agreement. This suggests that the POD modes actually represent the same flow structure at the same location.

Figure 7 shows a snapshot and its reconstruction using the two first POD modes. The snapshot has been selected by looking for snapshots where only one mode (in this case mode 2) has a large coefficient (a_2) as found by eq. (6), while the rest of the first few coefficient take values relatively close to zero. This selects a snapshot where POD mode 2 can be seen in a "clean" form. However, most other snapshots with a high positive value of the coefficient a_2 are similar to the snapshot in figure 7. The snapshot shows how a wake vortex has separated from the jet core. There is a positive velocity component in the core of the vortex. The vortex is therefore "tornado like". Near the upper edge of the jet core, (where $(x/D, y/D) \approx (0.5, 0.5)$) a new vortex is being created in interaction between the jet core and the crossflow. The reconstruction in figure 7 shows the effect of adding POD mode 2 to the mean flow. Here, the two vortices from the snapshot are clearly captured. This shows that the pattern in the snapshot is not a random phenomenon, but is occurring frequently.

The POD analysis presented from the LES has been made in planes corresponding to the

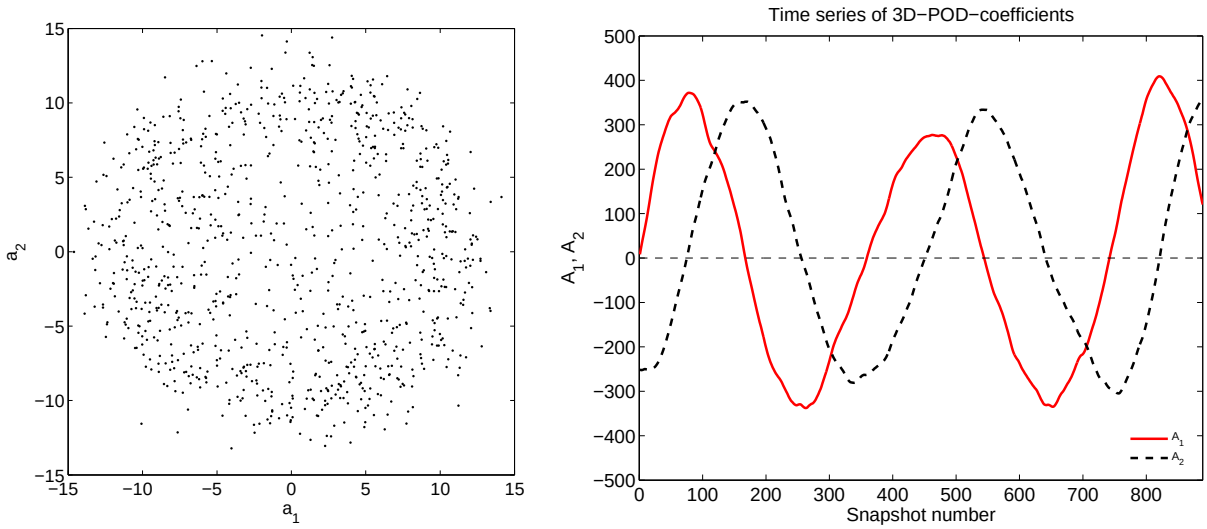

Figure 8: Coefficients a_1 and a_2 in the $y = 0$ plane for 1000 PIV snapshots (left) and for and LES times series (right).

PIV plane measured. In [9], the POD analysis has also been performed on a rectangular volume containing the two planes presented in the present paper. This analysis results in POD modes that agree well with the results from POD on planes. This shows that POD done on planes agree will with the "true" three-dimensional analysis as long as the plane contains the important phenomena in the flow.

Figure 8 shows a scatter plot of the coefficient for the first two POD modes in the $y = 0$ plane for the 1000 snapshots used in the analysis. The snapshots clearly fall in a circular distribution. This suggests that the coefficient (a_1, a_2) might tend to move along a circle, i.e. follow cosine and sine functions using time as parameter. The coefficients from time resolved snapshots from the three-dimensional POD analysis of LES are also shown figure 8. This plot confirms the assumption. Animation made with (a_1, a_2) following cosine and sine based functions do indeed show how vortices are continuously being created and shed downstream in the wake of the jet.

6 Conclusions

The snapshot POD analysis has been applied successfully on both PIV measurements and LES calculations of a turbulent jet in cross flow. In both cases, two important dynamical flow structures are identified: the wake vortices and the jet shear-layer vortices. The results show that these structures have almost identical shape and dynamics for the two realizations of the flow.

It is interesting to note that even though the POD is made only in a plane (as provided by stereo PIV) and thus only intersects the flow structures present, the POD analysis does capture the important structures. We also see that planes that intersect each other finds POD modes that are in agreement with each other. This is confirmed by a full three-dimensional POD analysis of the LES data. Furthermore, a pair of POD modes are describing "shedding" processes of vortices. The vortices in such a POD mode pair are displaced half a vortex width between the modes. Using a coefficient variation following a cosines and sinus variation with time as parameter results in an animation of the vortex shedding process. Finally, it is interesting to note that the dynamical content in the dominating modes from PIV and LES in the $y = 0$ plane agree quite well despite the presented disagreements between mean velocities in the jet core.

We find that POD is a very useful method both for analysis and comparison of POD and

LES data. A further advantage with POD is that is does not require assumption of the flow structures as it is the case with e.g. conditional sampling.

References

[1] T. F. Fric and A. Roshko. Vortical structure in the wake of a transverse jet. *J. Fluid Mech.*, 279:1–47, 1994.

[2] R. M. Kelso, T. T. Lim, and A. E. Perry. An experimental study of round jets in cross flow. *J. Fluid Mech.*, 306:111–144, 1996.

[3] T. T. Lim, T. H. New, and S. C. Luo. On the development of large-scale structures of a jet normal to a cross flow. *Phys. Fluids*, 13(3):770–775, March 2001.

[4] Knud Erik Meyer, Jakob M. Pedersen, and Oktay Özcan. A turbulent jet in crossflow analysed with proper orthogonal decomposition. *J. Fluid Mech.*, 2007. (accepted for publication).

[5] J. A. Michelsen. Block structured Multigrid solution of 2D and 3D elliptic PDE's. Technical Report AFM 94-06, Technical University of Denmark, 1994.

[6] N. N. Sørensen. *General Purpose Flow Solver Applied to Flow over Hills*. PhD thesis, Risø National Laboratory, Roskilde, Denmark, 1995.

[7] T.S. Lund, Xiaohua Wu, and K.D. Squires. Generation of turbulent inflow data for spatially-developing boundary layer simulations. *Journal of Computational Physics*, 140(2):233–258, 1998.

[8] P. Sagaut. Numerical simulations of separated flows with subgrid models. *Rech. Aero.*, pages 51–63, 1996.

[9] Dalibor Cavar. *Large Eddy Simulation of Industrially relevant Flows*. PhD thesis, Department of Mechanical Engineering, MEK - DTU, 2006.

[10] Oktay Özcan and Poul S. Larsen. An experimental study of a turbulent jet in cross-flow by using LDA. Technical Report MEK-FM 2001-02, Department of Mechanical Engineering, Technical University of Denmark, 2001.

[11] J. L. Lumley. The structure of inhomogeneous turbulent flow. In A. M. Yaglom and V. I. Tatarski, editors, *Atmospheric Turbulence and Radio Wave Propagation*, pages 166–178. 1967.

[12] L. Sirovich. Turbulence and the dynamics of coherent structures. Part I: Coherent structures. *Quart. Appl. Math.*, 45(3):561–571, 1987.

[13] Keinosuke Fukunaga. *Introduction to Statistical Pattern Recognition*. Academic Press, 2nd edition, 1990.

[14] Philip Holmes, John L. Lumley, and Gal Berkooz. *Turbulence, coherent structures, dynamical systems and symmetry*. Cambridge monographs on mechanics. Cambridge University Press, 1998.

[15] Jakob M. Pedersen. *Analysis of Planar Measurements of Turbulent Flows*. PhD thesis, Department of Mechanical Engineering, Technical University of Denmark, 2003.

[16] J.C.R. Hunt, A.A. Wray, and P. Moin. Eddies, stream and convergence zones in turbulent flows. Technical report, Center for Turbulence Research, NASA–Ames Research Center and Stanford University, California, USA, 1988.